Engineering Structures 225 (2020) 111321

Contents lists available at ScienceDirect

Engineering Structures

journal homepage: www.elsevier.com/locate/engstruct

Probabilistic seismic vulnerability and loss assessment of a seismic resistance bridge system with post-tensioning precast segmental ultra-high performance concrete bridge columns

Shuai Li [a,b,1], Taiyi Zhao [a,1], M. Shahria Alam [b], Zhao Cheng [a], Jing-quan Wang [a,*]

[a] Key Laboratory of Concrete and Prestressed Concrete Structures of Ministry of Education, School of Civil Engineering, Southeast University, Nanjing, Jiangsu, PR China
[b] School of Engineering, The University of British Columbia, Kelowna, BC, Canada

ARTICLE INFO

Keywords:
Highway bridges
Ultra-high performance concrete
Precast segmental column
Monolithic column
Performance-based engineering
Residual drift
Unbonded post-tensioning

ABSTRACT

Precast segmental ultra-high performance concrete (UHPC) columns with post-tensioned (PT) tendons can effectively protect the compression toe from damage and enhance energy dissipation (ED) capacity of column compared to conventional segmental concrete columns. Extensive experiments and numerical studies have been carried out to explore the cyclic response of segmental UHPC columns in the existing literature; however, the effect of such novel columns on the seismic safety of bridge structures has not been thoroughly understood. This study aims to numerically assess the seismic fragility and seismic life-cycle loss of bridge structures supported by the precast segmental UHPC columns. For comparison, the seismic performance of the same bridge with monolithic reinforced concrete (RC) piers are also evaluated. Here, three-dimensional (3D) numerical models are generated to simulate these two bridge types. A performance-based earthquake engineering (PBEE) framework is used to evaluate and compare their seismic performance. The segmental UHPC column model is validated with the previous experimental studies. The validated model is combined into the whole bridge. Numerical results showed that the precast segmental UHPC bridge experiences similar peak acceleration and larger peak displacement in comparison to the monolithic RC bridge. The segmental UHPC bridge pier experiencing lower residual deformation can effectively reduce the damage probability and life-cycle loss of a bridge compared to the conventional monolithic RC pier. Under the design event (2475-year return period) and maximum considered event (5000-year return period), the expected losses of the segmental bridge in the lifetime were approximate 92% and 84% of that of the monolithic bridge, respectively. The segmental UHPC bridge has a noticeable economic benefit when such a bridge is constructed in regions of high seismicity.

1. Introduction

During past earthquakes, many highway bridges with RC piers experienced a large unrecoverable residual drift yet not failed and had to be demolished and reconstructed [1]. Researchers and practicing engineers have made a consensus that the residual displacement of the bridge piers causes serious consequences on the functionality of RC bridge structures after an earthquake [2,3]. For mitigating the residual displacement of RC piers under earthquakes, various high-performance seismic resistance bridge systems with self-centering properties have been developed, such as PT precast segmental columns and shape memory alloy (SMA) reinforced bridge piers [4–6]. Unbonded PT precast segmental columns, as a kind of accelerated bridge construction, are more and more widely used due to high-quality control of fabrication, superior self-centering capacity, lesser environmental impact, and negligible residual displacement [7–10]. However, conventional precast segmental RC columns have two major problems. The first problem is that the opening and closing of the joints easily causes local damage at the compression toe. The second one is that their energy dissipation capacity is limited [11,12].

Currently, the application of a segmental bridge is usually limited in regions of low seismicity. For expanding their application in regions of high seismicity, many researchers have attempted to mitigate their seismic damage under strong earthquakes. Some approaches have been

* Corresponding author.
E-mail addresses: shahria.alam@ubc.ca (M.S. Alam), wangjingquan@seu.edu.cn (J.-q. Wang).
[1] Shuai Li and Taiyi Zhao have the same contribution in this study.

https://doi.org/10.1016/j.engstruct.2020.111321
Received 26 March 2020; Received in revised form 13 July 2020; Accepted 8 September 2020
Available online 25 September 2020
0141-0296/© 2020 Elsevier Ltd. All rights reserved.

proposed to avoid local concrete spalling at compression toe in a segmental column. For example, the stirrups, fiber-reinforced polymer (FRP), or steel jackets were proposed to confine part of the column or the whole column [13–18]. Some researchers utilized steel plates at the rocking interfaces or advanced materials in the plastic–hinge region [19–22]. Additionally, the segmental columns possess poor energy dissipation capacity (ED) due to the discontinuity of the steel reinforcements. To enhance their seismic ED capacity, various ED devices were developed. These devices can be divided into two types, consisting of internal devices (such as mild steel bars, SMA bars) and external devices (such as steel dissipater, aluminum bars, etc.) [15,20,23–30].

Recently, a new cementitious material, UHPC, has been developed. This new material has significant advantages including large strength, high ductility, and superior durability [31–33]. Previous researches have proved that UHPC can be ideally used in bridge columns located in high seismic regions [34–42]. However, considering its high cost compared to normal concrete, UHPC is used in critical regions of a structure only and their application in bridge engineering is still rare. For example, UHPC has been used as joint fill material between precast components or as materials for bridge foundation or girder elements. Considering its superior properties, the use of UHPC in the plastic hinge region can effectively avoid the cover spalling or crushing of a bridge pier. Binard [43] proposed that segmental UHPC columns can be promoted in bridge construction. Researchers, such as Ichikawa et al. [34], Yang and Okumus [11] experimentally and numerically investigated the seismic behavior of UHPC precast segmental columns with unbonded PT tendons. Although their seismic behavior has been thoroughly investigated at the component level, the effects of such segmental columns on a bridge structure at the system level have not been investigated in detail. To the authors' best knowledge, the studies on the seismic safety of precast segmental columns in a bridge system are still limited. For instance, Sideris et al. [44] experimentally explored the seismic behavior of a bridge system with precast segmental RC piers. Zhao et al. [45] performed numerical studies to investigate the seismic responses of precast segmental bridges. Lee and Billington [46] analyzed the seismic fragility and evaluated the economic loss of a bridge system supported by self-centering, post-tensioned RC columns in a PBEE framework. However, there is no study directly on exploring the seismic performance of a bridge supported by segmental UHPC columns at the system level. In this regard, it is vital to demonstrate the overall safety of the bridge impacting by the segmental UHPC columns under destructive (strong) seismic events.

2. Motivation and objective

Previously, the present authors [47,48] carried out a series of experiments to explore the cyclic response of the precast segmental UHPC columns with unbonded PT tendons. The results showed that such a novel column possessed higher allowable damage capacity and energy dissipation properties compared to the conventional precast segmental RC column. Only limited spalling without clear cracking was detected on the specimens' surface. The novel segmental columns presented excellent self-centering capacity after unloading and low residual deformation was observed. However, the impact of such columns on the system-level performance of a bridge has not been discussed in detail. Besides, the decision-makers have not yet recognized the lifetime benefit of such a bridge with segmental UHPC columns because of the higher initial cost of UHPC materials. Also, no study has been conducted on evaluating the economic loss for supporting decision making. Hence, it is necessary to perform a comprehensive performance-based assessment for successfully implementing such novel columns in a bridge.

This study aims at elucidating the possible benefit of segmental UHPC columns in the bridge design and hazard mitigation process. The system-level vulnerability and life-cycle performance of a highway bridge with segmental UHPC columns are evaluated to achieve this objective. First, a 3D finite element column model is generated to describe the hysteretic characteristics of segmental UHPC columns, which is validated against the experimental results. Then, a benchmark continuous bridge is taken as a reference bridge. The structural responses and vulnerability of the bridges with segmental UHPC piers and conventional monolithic RC piers are investigated. Finally, the economic impacts on the life-cycle performance of the bridge are estimated considering the direct and indirect loss.

3. Experimental studies and simulation of precast segmental UHPC columns

The present authors [47] have investigated the cyclic responses of three precast segmental unbonded post-tensioned UHPC columns through a cyclic-loading test. The specimens have a square hollow cross-section. The dimension of the cross-section is 500 mm × 500 mm and its thickness is 120 mm (see Fig. 1). Three components including a cap, three segments, and a foundation are assembled into one specimen. All these three components were manufactured with UHPC. The same height of 600 mm was set for each segment. The material properties of the UHPC were experimentally measured. The compressive strength and tensile strength were 124.3 MPa and 6.7 MPa, respectively. Eight strands with a diameter of 15.2 mm were used as the unbonded PT tendons. Eight mild steel bars with two different diameters (16 or 22 mm) were chosen as energy dissipation (ED) bars. The average yield strength of the ED bars was 447.3 MPa. Thirty-two 12 mm diameter steel bars were chosen as the longitudinal reinforcement, corresponding to a reinforcing ratio of 1.98%. 6 mm diameter steel bars with a center-to-center spacing of 50 mm were used as the transverse reinforcement. The yield strength of steel reinforcements is 566.7 MPa. The applied gravity load, P_G, was 1000 kN. Two axial load ratios were considered for the specimens in the experimental test program, i.e. 0.09 and 0.12. To reduce the initial cost and promote its application, a new type of UHPC material with river sand and coarse aggregate proposed by Liu et al. [49] was used to manufacture these specimens. The previous study has demonstrated that the properties of the new UHPC were similar to that of the UHPC without river sand and coarse aggregate [49].

A numerical approach is considered to estimate the seismic fragility of the investigated structural components and system in this study. Hence, it is necessary to validate the efficiency and accuracy of the numerical results. Here, a numerical model is built using OpenSees [50] to capture the hysteretic behavior of segmental UHPC columns. For validating the efficiency of the modeling technique in predicting the seismic hysteretic behavior, comparisons are made with experimental results. The specimen S-1 is taken as a case study. For specimen S-1, the PT force is designed as 400 kN. The ED bars have an unbonded length of 150 mm. A lumped mass is applied at the pier cap to represent the gravity load (see Fig. 1b). The top segment is connected with the pier cap using the RigidLink element. The nonlinear mechanical properties of each segment are simulated by fiber-based nonlinear beam-column elements. The unconfined and confined UHPC are modeled by Concrete 02 considering different material properties (see Table 1). A uniaxial Giuffre-Menegotto-Pinto steel model is considered to simulate the behavior of the reinforcements. The mechanical behavior of the PT tendons is described using a truss element. The detailed material properties of UHPC, steel reinforcement, and PT tendons in the FE model can be found in Wang et al. [47,48]. The prestressed strands are rigidly connected with the cap by RigidLink elements, as shown in Fig. 1b. In the specimen, the ED bars include two parts, i.e. the unbonded and bonded part. According to the previous studies [12,25], the unbonded part experiences plastic deformation and the bonded part remains elastic under lateral cyclic loading or earthquake excitations. In this regard, the unbonded ED bars in the FE model are modeled using truss elements as shown in Fig. 1b. The unbonded ED bars are rigidly connected with the pier using the RigidLink elements. The segment with bonded ED bars is modeled using fiber-based nonlinear beam-column elements. The previous experimental results [25,47] revealed that the opening at the

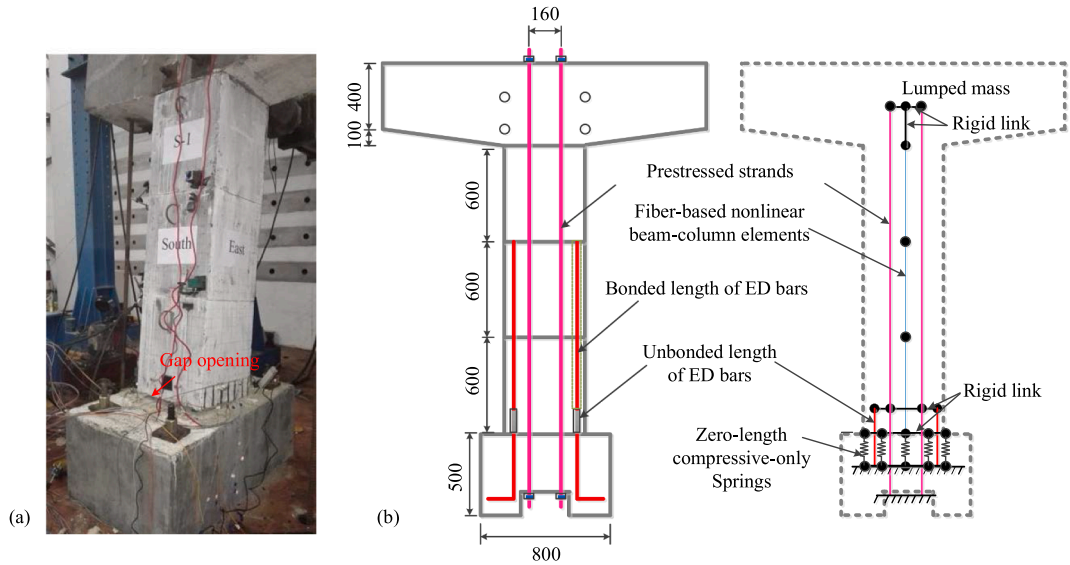

Fig. 1. Details of the (a) test specimen (S-1) [47], and (b) finite element model.

Table 1
Properties of the bridge.

Component	Material	Property	Value	Unit
Pier	ConventionalConcrete	Unconfined compressive strength, f_{uc}	30	MPa
		Confined compressive strength, f_{cc}	36.8	MPa
		Tensile strength	0	MPa
		Strain at peak stress, $\varepsilon_{cu,uc}$	0.2	%
	UHPC	Unconfined compressive strength, f_{uc}	124.3	MPa
		Confined compressive strength, f_{cc}	152.5	MPa
		Tensile strength	6.7	MPa
	Reinforcing Steel	Elastic modulus	200	GPa
		Yield stress, f_y	330	MPa
		Yield strain, ε_y	0.17	%
		Ultimate stress, f_u	455	MPa
		Ultimate strain, ε_u	0.31	—
Expansion Bearing	—	Yielding strength, F_s	370	kN
	—	Initial stiffness, k_e	123	kN/mm
	—	Friction coefficient, μ	0.2	—
Abutment	—	Stiffness, k_{abut}	164	MPa
	—	Passive pressure force, P_{bw}	1845	kN
Shear key	—	Concrete yield force, V_c	632	kN
	—	Yield deformation, Δ_n	17.6	Mm
	—	Ultimate deformation, Δ_{cu}	57.6	Mm
	—	Steel yield force, V_s	666	kN
	—	Yield deformation, Δ_y	4	Mm
	—	Ultimate deformation, Δ_u	105.3	mm

bottom joint was much larger than that of the other middle joints. Hence, the opening at the middle joints is ignored in this FE model and the compression-only elements are considered at the bottom joint only. Each segment is modeled with fiber-based nonlinear beam-column elements. A series of zero-length compression-only springs are used to model the opening and closing of the bottom joint (see Fig. 1b). The stiffness of these compression-only elements (see Fig. 1b) can be expressed as [51]

$$E = \frac{E_c A_g}{L \times n}\theta \tag{1}$$

where E_c is the elastic modulus of UHPC; A_g is the cross-section area of the pier; L is the clear height of the pier; n is the number of zero-length elements; θ is the empirical coefficient, which ranges from 1.0 to 2.0 following the work of Si et al. [51].

The segmental UHPC column (specimen S-1) is taken as an example in this study. In the FE model, the fracture of ED bars is considered as the failure criterion of the segmental UHPC columns. This is because all the specimens in the experimental tests eventually experienced fracture of ED bars where the tests were performed by the same authors [47]. The same loading history was used for both the experimental tests and numerical simulations. The lateral cyclic loading was applied at the top of the pier from 0.25% to 8% drift ratio. When the fracture of the ED bars is observed, the simulation was stopped. The test and numerical results of the hysteretic curves for specimen S-1 are compared and shown in Fig. 2. It can be observed that the initial yield of the specimen and fracture of the ED bars from the FE model match well with those of the tested specimen. Since UHPC is used in the column, the concrete crushing is not observed in the FE model. The same phenomenon was observed during the tests where only concrete spalling was observed at the bottom joint and no flexural or shear cracks were observed on the surfaces of each segment. Besides, the joint opening could be accurately predicted by the proposed model as shown in Fig. 2b. In this regard, the hysteretic behavior of the segmental UHPC columns can be accurately captured by the FE model. Here, it should be mentioned that in a latest study by one of the authors [52], the accuracy and efficiency of the proposed model is also validated against the experimental results by ElGawady et al. [53], Palermo et al. [23], and Mander et al. [13].

4. Case study: A benchmark bridge

For more generality, a typical two-span continuous benchmark bridge is considered as the reference. The seismic behavior of the bridge has been numerically investigated in the studies of [54,55]. Without considering the same location in the previous works, it is assumed that the bridge is located in Western Canada on stiff soil in the present study. Here, it should be mentioned that such continuous bridges are widely

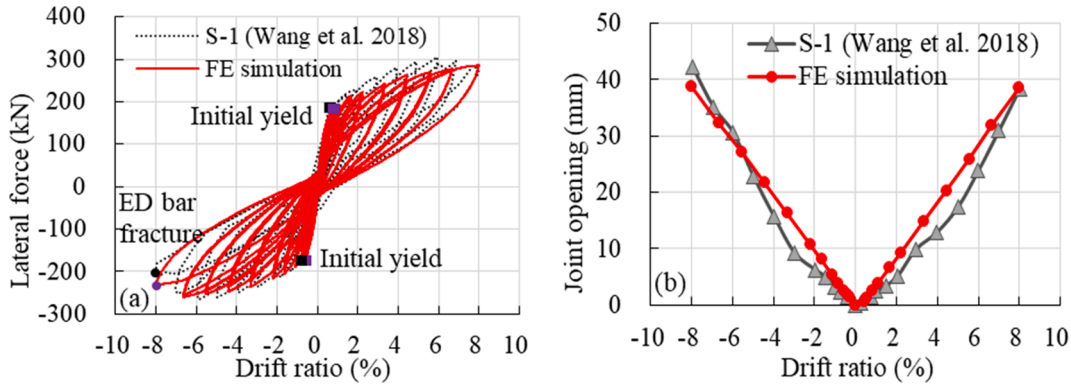

Fig. 2. Comparison of the numerical hysteretic curve and joint opening with the test results (specimen S-1) in Wang et al. [47].

constructed in the transportation network of Western Canada (more than 20%) based on the investigation by Siddiquee and Alam [56]. Among these continuous bridges, the most common-used number of spans is two or three.

4.1. Bridge description and finite element modeling

The considered continuous bridge has two equal spans with each span length of 20 m (see Fig. 3). The superstructure is an RC two-box girder. Two abutments and an RC pier are used to support the concrete girder. The RC pier has a solid square cross-section and its clear height is 7.0 m. The dimension of the solid cross-section for the pier is 0.9 m × 0.9 m. The space of the expansion joint between the girder and abutment is 0.1 m. The pier is reinforced with 32-M28 steel rebars. A total of two fixed bearings and four conventional expansion bearings are installed at the pier and abutment locations, respectively. The compressive strength of the normal concrete is 30 MPa. The steel reinforcement has a yield strength of 330 MPa. More information on the bridge is available in the references [54,55].

In this study, two different column types are used to explore the impact of the segmental UHPC columns. One bridge is supported by the monolithic RC pier (the reference bridge). For another one, the segmental UHPC pier is used to replace the monolithic RC pier. UHPC has a higher initial cost compared to conventional concrete. To compensate for higher initial cost, the authors have incorporated river sand and coarse aggregate into UHPC and used hollow cross-section in bridge piers. In the prototype bridge, a solid cross-section is used for the bridge pier. In this study, a hollow cross-section is considered for the segmental UHPC pier. The UHPC material has a compressive strength of 124.3 MPa and the tensile strength of 6.7 MPa. The following section provides a detailed design procedure to properly design such a novel bridge pier. The present authors [47] have experimentally demonstrated

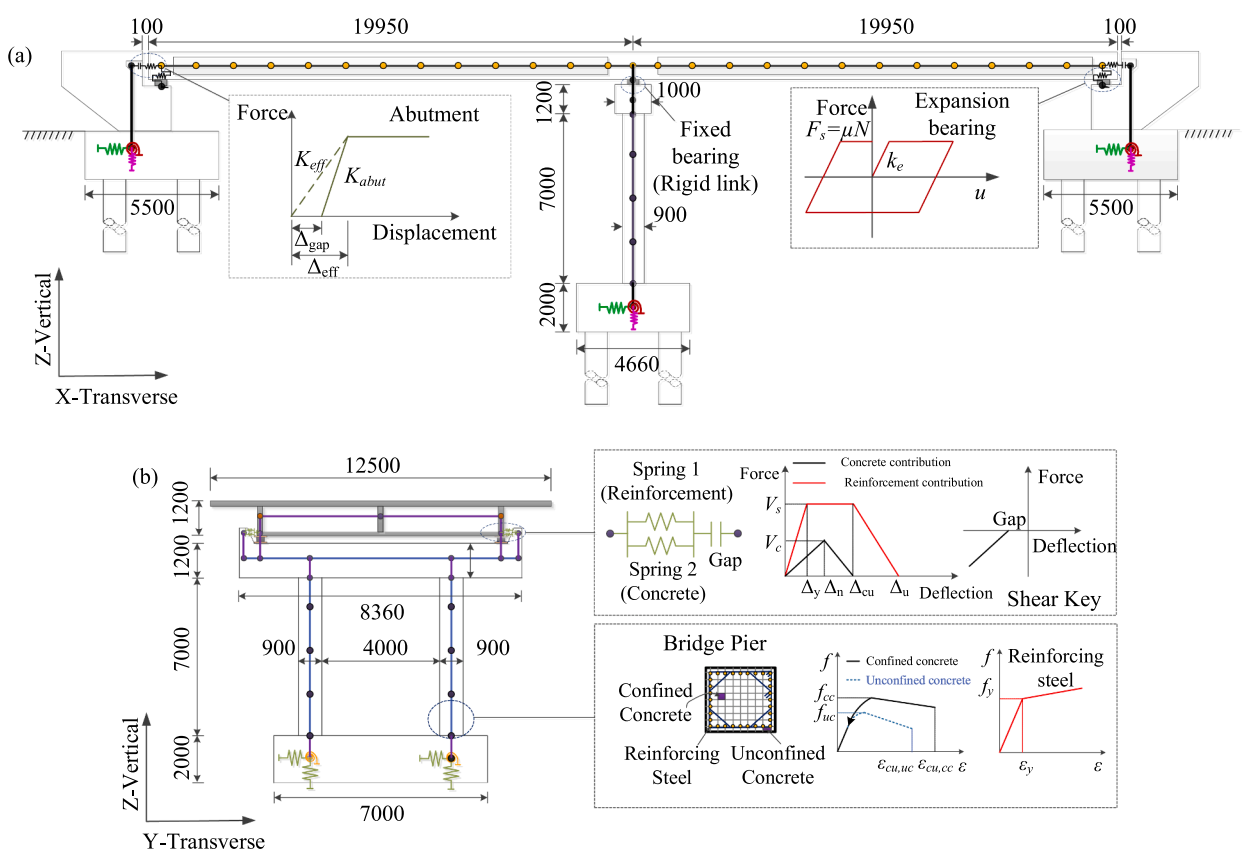

Fig. 3. (a) Configuration for the prototype bridge and (b) elevation view of the pier (unit: mm).

that the precast segmental UHPC columns possess good energy dissipation capacity, low residual drift, and superior damage tolerance ability. In the studied bridge, the axial load ratio of the bridge pier is 0.15. Note that the axial load ratios of both the specimens in the experimental test program and the piers in the bridge are in the range of the common-used axial load ratio for highway bridges (i.e. from 0.03 to 0.2). The axial load ratio may have a significant influence on the behavior of the bridge pier. The authors have thoroughly discussed the effect of the axial load ratio in a latest study [12]. The results showed that a larger axial load ratio is beneficial in improving the self-centering capacity of the segmental UHPC column. Besides the axial load ratio, several key design parameters, such as ED bar ratio, aspect ratio, unbonded length of ED bars, etc., are also discussed in the same study. Considering the space limitation of the study, the effects of these design parameters are not discussed in the current study.

A total of 1030.5 m^3 concrete and 91.9 tons of steel are used to build the reference bridge. In the novel bridge, 8.1 m^3 UHPC is used to manufacture the bridge piers. The price of the UHPC material with river sand and coarse aggregate is about \$2200/m^3. Considering the costs of the material, fabrication, and formwork, the total costs during the construction for the two bridges are \$648,429 (the prototype bridge) and \$665,439 (the segmental bridge), respectively. It can be found that the segmental UHPC pier increases the construction cost by only 2.6% compared to the prototype bridge. It should be mentioned that the excavation cost, labor cost, etc. may impact the evaluation of the initial cost of the bridge. After giving more information, the construction cost can be accurately estimated.

Two bridges are considered in this study, i.e. one bridge is the prototype bridge and another one is the bridge supported by the segmental UHPC piers. The numerical models of the two bridges are developed and used to compare their seismic performance under strong earthquakes. The elastic beam-column elements are used to simulate the superstructure and pier cap. The pounding effects of deck-abutment are described by the bilinear contact elements. The bridge piers are simulated utilizing the fiber-based nonlinear beam-column elements. In the pier model, the cover, core concrete, and steel reinforcements are modeled using different stress–strain relationships (see Fig. 3 and Table 1). In the above section, the modeling approach for the precast segmental UHPC columns has been confirmed against the test results of the specimen. In this section, the same modeling approach is used to simulate the precast segmental UHPC bridge piers. The behavior of the abutment is described using the method provided in the Caltrans (see Fig. 3) [57]. Linear spring elements are used to model the foundation. The stiffness of each spring is determined depending on FHWA [58]. The stiffnesses of the translational (k_x, k_y, and k_z) are 1.14×10^4, 1.19×10^4, and 1.54×10^4 kN/mm, respectively. The corresponding values of the rotational springs ($k_{\theta x}$ and $k_{\theta y}$) are 7.76×10^{10} and 1.51×10^{11} kN·mm/rad, respectively. The elastic–plastic model with the same mechanical properties used in reference [54] is considered to describe the constitutive model of the expansion bearings. The product of the friction coefficient (μ) and normal force (N) acting on the bearing are set as the yield strength of the bearing (1850 kN $\times$ 0.2 = 370 kN). The frictional coefficient and initial stiffness are 0.2 and 123.0 kN/mm, respectively. A rigid link is used to simulate the fixed bearings at the pier location, i.e., the girder is rigidly connected to the bridge pier for both longitudinal and transverse directions. The hysteretic behavior of the shear key is described using an elastic–plastic model [59]. In this model, the constitutive behavior of the shear key is simulated using two parallel nonlinear springs in series with a gap. The damping ratio of the bridge is assumed 5% according to the Canadian Highway Bridge Design Code [60]. The models for the abutments, expansion bearings, fixed bearing, pier, and shear keys have been provided in Fig. 3. The corresponding material properties are tabulated in Table 1.

4.2. Design of precast segmental UHPC columns

As mentioned earlier, since the prototype pier in the reference bridge has a solid cross-section, a precast segmental UHPC bridge pier with a hollow cross-section should be properly designed. Here, a design procedure is developed to design the precast segmental UHPC columns with post-tensioned tendons.

Lee and Billington [46] compared the seismic performance of the conventional monolithic RC piers with the precast segmental RC piers. For directly comparing their performance subjected to earthquake excitations, they suggested that the designed precast segmental columns should have the same dimension with the monolithic RC columns. Also, their stiffness and strength should remain similar. Following their suggestions, the design procedure of the precast segmental UHPC columns

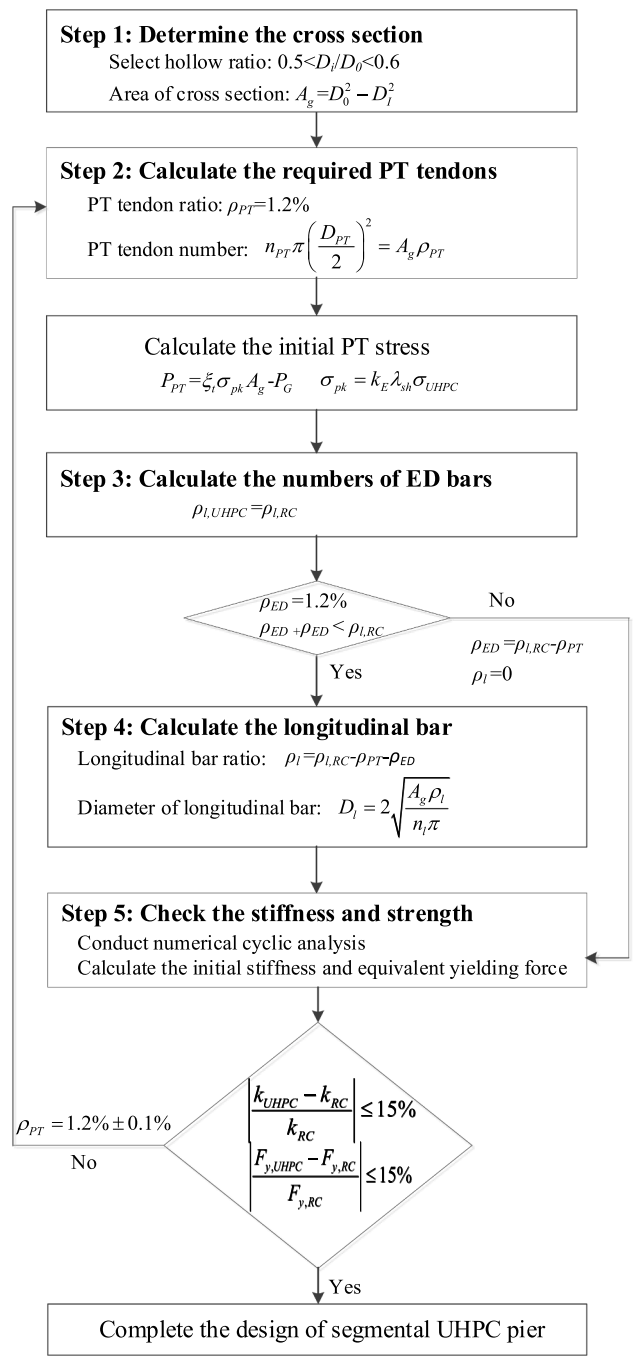

Fig. 4. Flow chart of the design procedure for the segmental UHPC column.

with a flowchart (see Fig. 4) is provided as follows. Here, it should be mentioned that unlike the seismic design of a regular RC column, the design approach of a precast segmental UHPC column has not been specified in the current seismic design codes. Hence, the proposed procedure can aid the designers in designing such a novel bridge column.

Step 1: Determine the cross-section of the precast segmental UHPC hollow pier

The hollow ratio calculated by the ratio of the inside to outside dimension of the hollow cross-section (D_i/D_0) is considered to determine the dimensions of the cross-section. A hollow pier database collected by Wang et al. [48] showed that the most common-used hollow ratio ranges from 0.5 to 0.6. Hence, the inside and outside dimensions are set as $D_i = 480$ mm and $D_0 = 900$ mm, respectively. The corresponding hollow ratio is 0.53.

Step 2: Calculate the required PT tendons and initial PT stress

A sensitivity study has been conducted to determine the optimal PT tendon ratio [12]. It was found that when the PT tendons have an area ratio (ρ_{PT}) of 1.2%, the self-centering property and ED capacity of the segmental UHPC column can be effectively balanced. Hence, 17.8 mm diameter seven-wire strands, i.e. $D_{PT} = 17.8$ mm, are used as the PT tendons. The resulting design uses 28PT tendons ($n_{PT} = 28$) with a total area of 6955 mm^2.

For comparing the two different columns at the same level, it is considered that the hollow pier has the same load-bearing capacity as that of the monolithic pier [46]. Here, a parameter, ξ_t, is defined to measure the load-bearing capacity of the pier section.

$$\xi_t = \frac{P_G + P_{PT}}{\sigma_{pk} A_g} \tag{2}$$

where P_{PT} is the initial PT force; σ_{pk} denotes the peak stress of concrete. The peak stress of UHPC can be determined by [12]

$$\sigma_{pk} = k_E \lambda_{sh} \sigma_{UHPC} \tag{3}$$

where σ_{UHPC} represents the compressive strength of UHPC; $\lambda_{sh} = 0.85$ is the shape factor; $k_E = 0.85$ is the modified factor. The compressive strength of UHPC with coarse aggregate is set as 124.3 MPa [47].

The load-bearing capacity of the monolithic bridge pier is 0.152. The initial prestress of PT tendons for precast segmental UHPC column is 607 MPa according to Eq. (3).

Step 3: Calculate the numbers of ED bars

After designing the PT tendons, the following criterion is considered to calculate the suitable number of ED bars. Namely, the precast segmental UHPC columns have a roughly similar reinforcement ratio with the monolithic columns ($\rho_{l,UHPC} = \rho_{l,RC}$) according to Sakai and Mahin's recommendation [61]. In this study, ED bars are considered to be continuous along with the whole height of the pier for enhancing the seismic resistance of the column (see Fig. 5).

$$\rho_{l,RC} = \rho_{l,UHPC} = \rho_{ED} + \rho_l + \rho_{PT} \tag{4}$$

where $\rho_{l,UHPC}$ and $\rho_{l,RC}$ are the reinforcement ratios of the precast segmental UHPC and monolithic column, respectively; ρ_l, ρ_{ED}, and ρ_{PT} are the ratios of the longitudinal bars, ED bars, and PT tendons, respectively.

Following the work of Wang et al. [12], when ρ_{ED} is set as 1.2%, the residual drift of the precast segmental UHPC pier will have an effective balance with the equivalent viscous damping. If the sum of ρ_{ED} and ρ_{PT} is larger than the reinforcement ratio of the monolithic column, $\rho_{l,RC}$, the longitudinal bar ratio, ρ_l, can be set as 0 and the ED bar ratio is suggested to be calculated as

$$\rho_{ED} = \rho_{l,RC} - \rho_{PT} \tag{5}$$

A total of twelve 28 mm diameter mild steel bars are used as the ED bars for the segmental pier. To ensure the ductility and ED capacity of the pier, an unbonded length of ED bars at the base of the bottom segment is suggested to be considered.

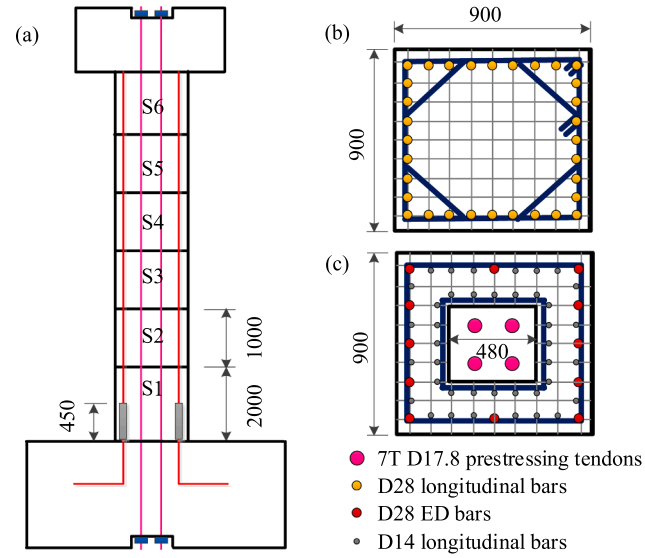

Fig. 5. Details of the designed segmental UHPC column (a) elevation of the segmental column; (b) cross-section of the monolithic column; (c) cross-section of the segmental column (mm).

Step 4: Calculate the longitudinal bars

After determining the ratios of ED bars and PT tendons, the longitudinal bar ratio, ρ_l, can be calculated according to Eq. (4). Here, the longitudinal bars refer to the longitudinal reinforcement inside each segment. They are not extended across the segment joints.

Then, the number of longitudinal rebars, n_l, can be determined based on the dimension of the cross-section of the pier and the requirement of the seismic design codes. Lastly, the diameter of the longitudinal steel bars, D_l, can be determined as

$$D_l = 2\sqrt{\frac{A_g \rho_l}{n_l \pi}} \tag{6}$$

According to Eqs. (4) and (6), forty 14 mm diameter steel bars are utilized as reinforcement bars.

Step 5: Check the stiffness and strength between the precast segmental UHPC column and monolithic column

As mentioned earlier, the two different bridge piers should have similar stiffness and strength to make them comparable at the same level. In this regard, a numerical cyclic analysis is conducted on the above designed segmental piers. The initial stiffness (k_{UHPC}) and equivalent yielding strength ($F_{y,UHPC}$) of the segmental UHPC column are compared with that of the monolithic RC piers (k_{RC} and $F_{y,RC}$).

$$-15\% \leqslant \frac{k_{UHPC} - k_{RC}}{k_{RC}} \leqslant 15\% \tag{7-1}$$

$$-15\% \leqslant \frac{F_{y,UHPC} - F_{y,RC}}{F_{y,RC}} \leqslant 15\% \tag{7-2}$$

If the difference is larger than 15%, the amounts of PT tendons and steel reinforcements in the above design should be varied using the initial design. Their optimum values can be determined by performing a series of cyclic analyses.

According to the proposed design procedure, the precast segmental UHPC column can be designed as illustrated in Fig. 5. The hysteretic curves of the two types of bridge pier associated with the envelope curves under cyclic loading are presented in Fig. 6. Table 2 lists the operational characteristics of these two columns, including the initial stiffness, k_{ini}, the equivalent yielding force F_y, the maximum lateral loading, F_{max}, the residual drift, D_{res}, self-centering ratio, SCR, dissipated energy, E_0, and equivalent viscous damping ratio, β. Here, β denotes the

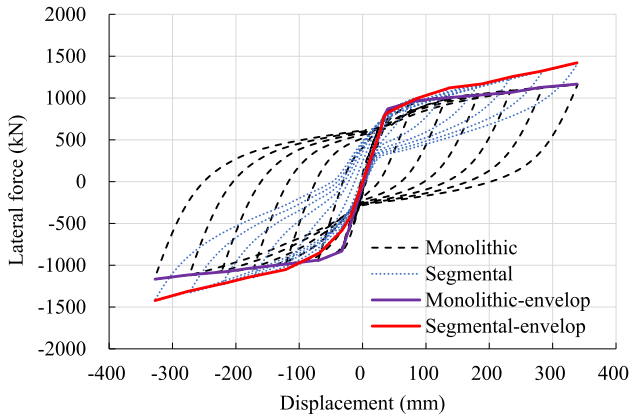

Fig. 6. Comparison of the hysteretic behavior of monolithic and segmental UHPC column.

Table 2
Property comparisons of monolithic and segmental UHPC columns.

Column type	k_{ini} (kN/m)	F_y (kN)	F_{max} (kN)	D_{res} (mm)	E_0 (kJ)	β (%)	SCR
Monolithic	24.3	787	1167	250	637	26.1	0.25
Segmental	22.7	782	1422	48	501	6.9	0.96

viscous damping ratio of the bridge column without considering the contribution of the bearings and abutments.

$$\beta = \frac{E_o}{2\pi K_{eff}\Delta_{max}^2} \tag{8}$$

where K_{eff} and Δ_{max} are the scant stiffness and amplitude of the cycle, respectively. The SCR represents the self-centering capacity and is defined as

$$SCR = 1 - \frac{\Delta_{zero}}{\Delta_{max}} \tag{9}$$

where Δ_{zero} is the horizontal displacement when force is zero.

For comparison, the cyclic responses of the segmental and monolithic bridge columns are shown in the same plot (see Fig. 6). It can be observed that the two columns have almost the same initial stiffness and yielding force with a small difference (less than 5%). In this regard, the two bridge systems can be directly compared according to the recommendations of Lee and Billington [46].

As observed from Fig. 6 and Table 2, the segmental UHPC column presents superior self-centering property due to the effects of PT tendons. The residual drift of the monolithic column decreases from 250 mm to 48 mm after using the segmental UHPC column. The self-centering ratio (SCR) increases from 0.25 to 0.96 (283% increase). However, the dissipated energy of the segmental UHPC column is lower than that of the monolithic RC column (21% reduction). The segmental UHPC column causes the equivalent viscous damping ratio to decrease from 26.1% to 6.9%. Another finding is that the stiffness of the monolithic column decreases when the drift ratio is larger than about 1.2%, while the segmental columns do not experience a stiffness degradation. The phenomenon can be explained that for the monolithic column, concrete damage and reinforcement yielding cause more severe strength degradation. The precast segmental UHPC column experiences negligible concrete damage because of the superior mechanical properties of UHPC.

Using the designed segmental UHPC bridge piers instead of the monolithic RC bridge pier, modal analysis is conducted to calculate the natural periods of the two bridges. The periods of the benchmark bridge and the bridge with the segmental UHPC columns are 0.274 and 0.279 s, respectively. The period of the benchmark bridge is almost the same as that of the one (0.277 s) presented in Zheng and Dong [54]. Since the two bridge columns have similar initial stiffness, the periods of the two bridge systems are almost the same.

4.3. Ground motion suite

In this study, the efficiency of the segmental UHPC columns is investigated to estimate the seismic damage of the bridge system under destructive earthquakes. Since the benchmark bridge is assumed to be located in Western Canada regions, the ratio of PGA to PGV ranges from 0.8 to 1.2 [62,63]. In previous studies, the authors have proved that the near-fault ground motions with unique characteristics have stronger influences on the seismic responses of the structures compared to the far-field ground motions [62,64,65]. Hence, 21 near-fault ground motions used in Ref. [62] are chosen to assess the life-cycle performance of the bridges under destructive conditions (high level of seismic activity). The magnitude (M_w) varies from 6.5 to 7.6 and the PGA values range from 0.13 g to 0.79 g. The selected ground motions are applied in both the longitudinal and transverse directions. The record characteristics are tabulated in Table 3. The 5% damped elastic acceleration response spectra are illustrated in Fig. 7. Note that this strategy can also be successful in conservatively evaluating the seismic performance of the bridges during far-field events. Further research is needed to validate the findings of this study for far-field events.

5. Methodology of performance-based earthquake engineering (PBEE)

A PBEE framework has been developed to assess and design the civil infrastructures by the PEER center. In the framework, various consequences, such as repair loss, downtime, etc. are considered. The framework encompasses four steps (see Fig. 8). In the first step, the seismic scenarios are determined according to the location and seismic design of the bridge. Here, the seismic scenarios associated with various frequencies and intensity measures (IMs) are determined according to hazard curves [66]. The PGA is selected as the intensity measure (IM) [54,67]. Then, in the structural analysis, Engineering Demand Parameters (EDPs) of structures can be determined by performing simulations on the numerical model of the bridge. An incremental dynamic analysis will be conducted to determine the correlation between the EDPs and the corresponding IMs. After determining IMs and EDPs, the damage probabilities of a structural component or system can be obtained by conducting vulnerability analysis. In the last step, the loss analysis is conducted to assess the economic loss of the bridge with segmental UHPC columns.

6. Comparative seismic responses of the prototype and novel bridges

The seismic responses of the two bridges are compared under strong earthquakes in this section. The deck displacement, D_{deck}, and deck acceleration, a_{deck}, and the hysteresis curves of the piers in the longitudinal direction are assessed through dynamic history analyses. The average values of each peak response are calculated and listed in Table 4. The average values of the operational characteristics of the bridge piers are also listed in the same table. The seismic responses of the abutments and expansion bearings are also attained from the structural analysis. For brevity, these time histories are not provided in this study.

6.1. Seismic responses of the deck

The time histories of the deck under two destructive earthquakes are illustrated in Figs. 9 and 10. The displacement and acceleration responses at the midspan location (left span) in the longitudinal direction are recorded. Table 4 lists the mean peak responses of the deck. Fig. 9

Table 3
Characteristics of near-fault ground motions.

No	Earthquake	Year	Magnitude (Richter)	Station component	Epicentral distance (km)	PGA (g)	PGV (cm/s)
1	Chi-Chi	1999	7.6	TCU065-E	2.5	0.79	115.0
2	Chi-Chi	1999	7.6	TCU071-E	5.8	0.53	52.3
3	Chi-Chi	1999	7.6	TCU074-E	13.5	0.38	44.9
4	Chi-Chi	1999	7.6	TCU078-E	8.2	0.45	40.2
5	Chi-Chi	1999	7.6	TCU079-E	11.0	0.59	70.5
6	Chi-Chi	1999	7.6	TCU084-N	11.5	0.43	48.1
7	Imperial Valley	1979	6.5	CHI012	7.3	0.27	24.9
8	Imperial Valley	1979	6.5	E08230	3.9	0.47	52.0
9	Imperial Valley	1979	6.5	E11230	12.6	0.38	44.6
10	Kobe	1995	6.9	KJM090	1.0	0.63	76.1
11	Kobe	1995	6.9	NIS090	7.1	0.46	38.3
12	Landers	1992	7.3	JOS000	11.0	0.27	27.6
13	Loma Prieta	1989	6.9	BRN000	10.7	0.46	51.4
14	Loma Prieta	1989	6.9	CLS090	3.9	0.48	47.6
15	Loma Prieta	1989	6.9	G02000	11.1	0.37	36.8
16	Loma Prieta	1989	6.9	SJTE225	14.7	0.28	28.2
17	Northridge	1994	6.7	LOS070	12.4	0.47	41.1
18	Northridge	1994	6.7	STC090	12.1	0.34	31.5
19	Northridge	1994	6.7	PKC090	7.3	0.30	31.0
20	Northridge	1994	6.7	RO3000	10.1	0.28	25.3
21	Northridge	1994	6.7	GLE170	13.4	0.13	15.7

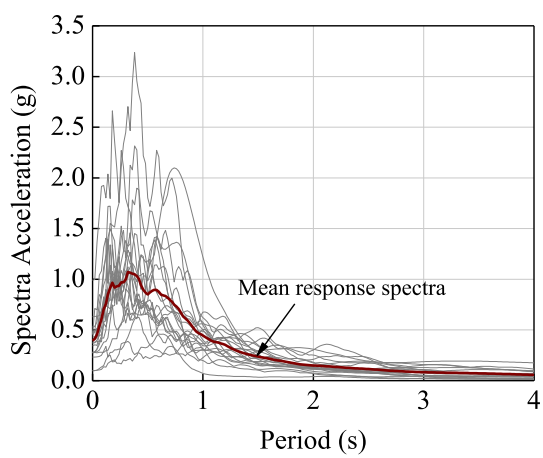

Fig. 7. 5% damped elastic acceleration response spectra along with the mean response spectrum.

shows that the deck in the novel bridge experiences negligible residual deformation after the earthquakes due to the superior self-centering capacity of the segmental UHPC piers. However, a large residual deformation of the deck in the prototype bridge with the monolithic piers is observed in Fig. 9. For example, the deck residual displacement under the Kobe earthquake decreases from 59.9 mm to 1.0 mm (98.3% reduction). The average value of the residual displacement is 7.79 mm for the bridge with the monolithic column. While using segmental UHPC columns, the corresponding mean value reduces to 1.43 mm, with the reduction ratio reaching 81.7% compared to that of monolithic columns. This phenomenon can be explained by the superior self-centering property of the segmental UHPC columns (see Fig. 11). Another finding from Fig. 9 is that the peak displacements of the deck in the segmental bridge are higher than those in the prototype bridge. The mean peak deck displacement increases from 43.5 mm (monolithic bridge) to 50.9 mm (segmental bridge) (17.1% increase). It can be explained by the lower energy dissipation capacity of the segmental UHPC columns compared to the monolithic RC columns (see Fig. 11). The two bridge systems have the same lateral stiffness, seismic force, and input seismic energy, however, the segmental UHPC columns dissipate less seismic energy and as a result, the deck experiences more vibrations. The same phenomenon is observed in the study of Zhao et al. [45].

The time histories of the deck acceleration for the two bridges are plotted in Fig. 10. It can be seen that the peak accelerations of the deck are almost the same for the two bridge structures. The average values of

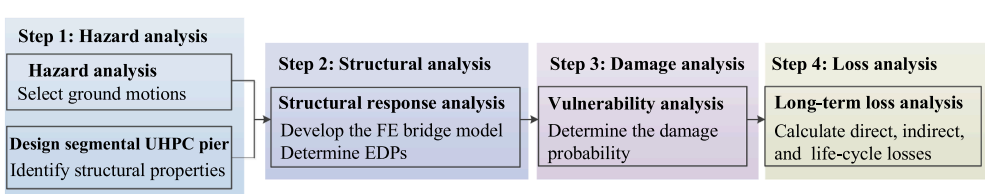

Fig. 8. Flowchart of the long-term loss assessment of a bridge with segmental UHPC columns.

Table 4
Operational characteristics of bridge deck and pier.

Bridge type	Deck			Pier			
	D_{deck} (mm)	a_{deck} (g)	D_{res} (mm)	D_{pier} (mm)	D_{res} (mm)	SCR (%)	E_0 (kJ)
Monolithic	43.5	0.52	7.79	42.2	7.78	0.82	57.5
Segmental (Δ) *	50.9	0.51	1.43	49.8	1.40	0.97	33.2
	17.1%	−1.2%	−81.7%	18.2%	−82.0%	19.2%	−42.2%

* Difference between the responses of the prototype bridge and innovative bridge.

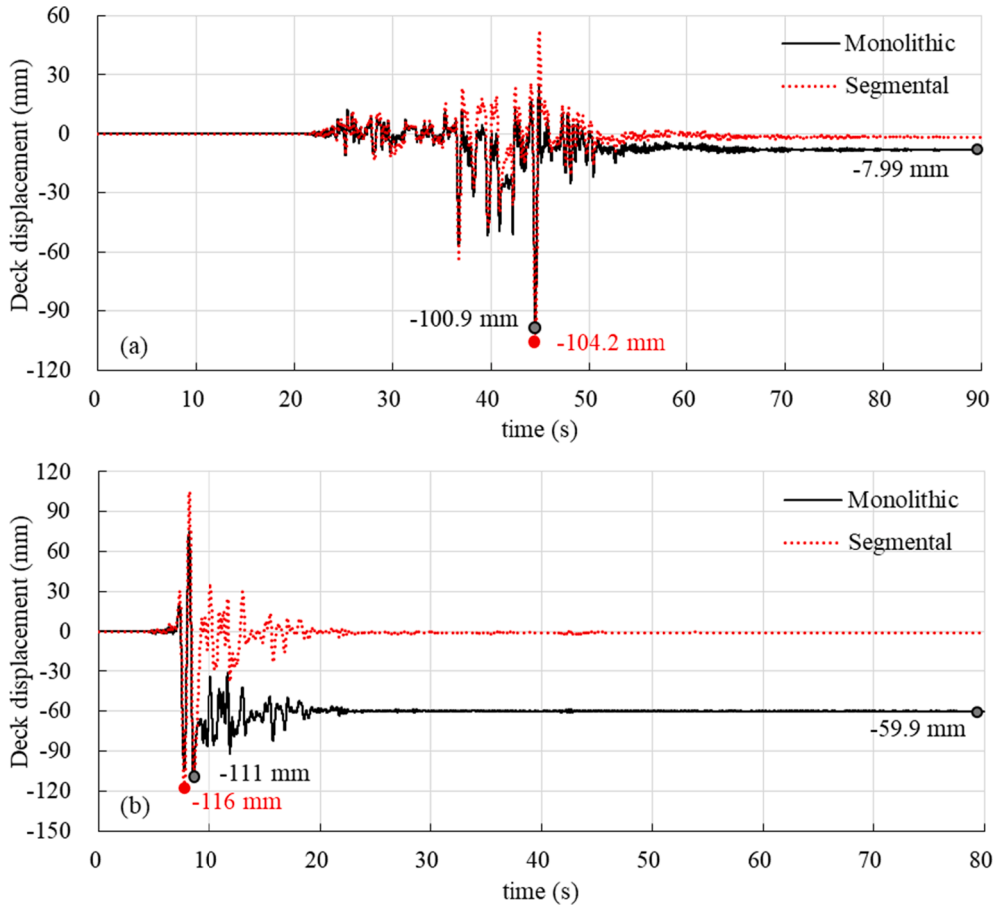

Fig. 9. Time history of deck displacement under (a) TCU079, ChiChi and (b) KJM090, Kobe.

the peak acceleration for the prototype and segmental bridges are 0.52 g and 0.51 g, respectively (see Table 4). It means that by replacing monolithic columns with segmental columns designed by the proposed procedure does not significantly increase the seismic force of the bridge structure.

6.2. Seismic responses of the pier

Fig. 11 depicts the longitudinal force–deformation relationship of the two bridge columns under the ChiChi and Imperial Valley earthquakes. It can be seen from Fig. 11 that the piers in the studied bridge may remain elastic or experience yielding of rebar under earthquakes. However, the rupture of the rebars is not observed under the considered earthquake excitations. When the piers experience plastic deformation, the monolithic pier has a larger residual deformation compared to the segmental UHPC column where the segmental UHPC column presents a superior self-centering capacity. Table 4 lists the average values of the operational characteristics for the piers under 21 near-fault ground motions. Compared to the monolithic RC columns, the segmental UHPC columns experience smaller residual displacement. The average residual displacement for the segmental UHPC columns decreases by 82% and the increase in the SCR is 19.2%. The mean peak displacement of the segmental UHPC column is higher than that of the monolithic column (from 42.2 mm to 49.8 mm). This phenomenon can be explained by the low ED capacity of segmental UHPC columns. As an example, the segmental UHPC columns lead to a 42.2% reduction in mean energy dissipation (from 57.5 kJ to 33.2 kJ) (see Table 4). It can be also observed from Tables 2 and 4 that the monolithic pier has two different values of SCR under cyclic loading and earthquake excitations. The value of SCR under cyclic loading is smaller than that under earthquake excitations. This phenomenon can be explained by the following fact. Compared to the cyclic loading (from 25 mm to 340 mm), the monolithic pier experiences smaller lateral displacement with an average value of 42.2 mm under earthquake excitations in the full bridge system (Table 4). Especially, under some earthquakes, the monolithic piers remain elastic (see Fig. 11b). This is the reason that the monolithic pier under earthquake excitations has a high SCR value. However, when the piers experience plastic deformation with the increase of the lateral displacement (see Figs. 6 and 11a), the SCR of the monolithic pier decreases due to the increase of the residual deformation. Hence, the self-centering capacity in piers may not be helpful to improve the performance of the whole bridge when the piers experience a small lateral deformation. However, under a destructive earthquake ground motion, the self-centering capacity of the piers will play an important role in mitigating the seismic damage of the bridge system.

7. Seismic vulnerability analysis of the conventional and novel bridges

The damage probabilities of each bridge component (i.e. bearing and pier) are expressed as follows.

$$P[DS|IM] = \Phi\left[\frac{bln(IM) - lnS_c + lna}{\sqrt{\beta_{D|IM}^2 + \beta_c^2}}\right] \tag{10}$$

The regression coefficients (a and b) can be derived from the regression analysis. The median estimate, S_c, and the corresponding conditional dispersion, β_c, associated with the structural capacity are determined based on the existing literature [2,71]. The conditional dispersion of the demand, $\beta_{D|IM}$, can be computed using Eq. (11).

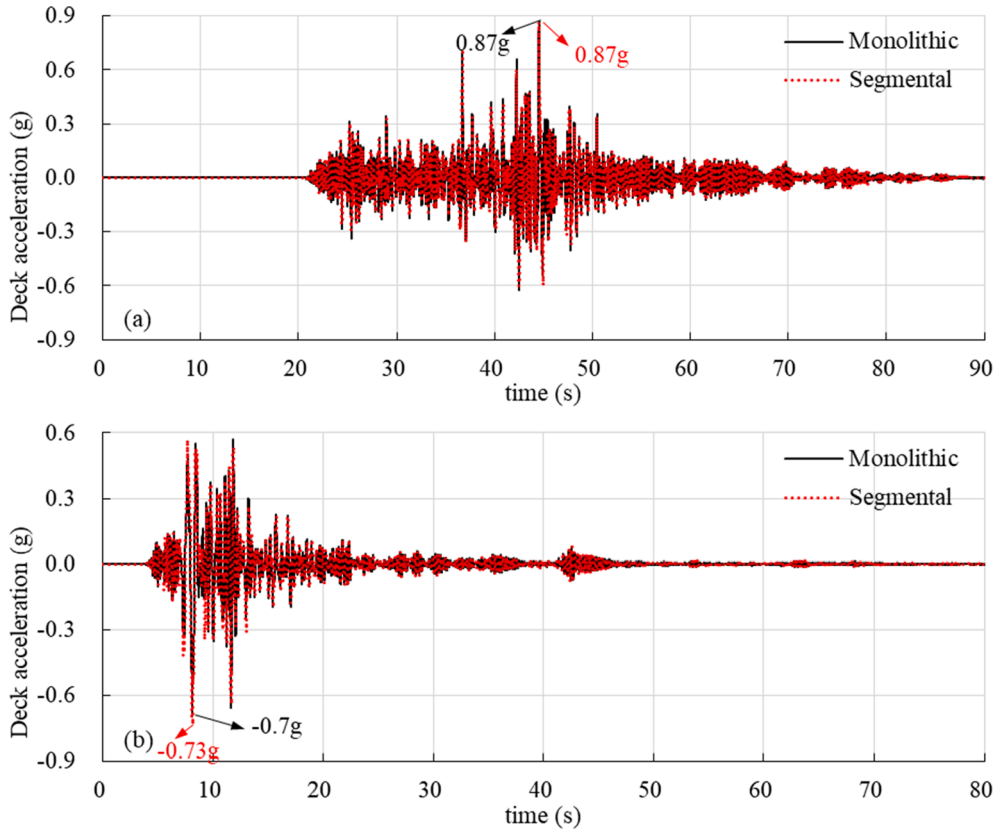

Fig. 10. Time history of deck acceleration under (a) TCU079, ChiChi and (b) KJM090, Kobe.

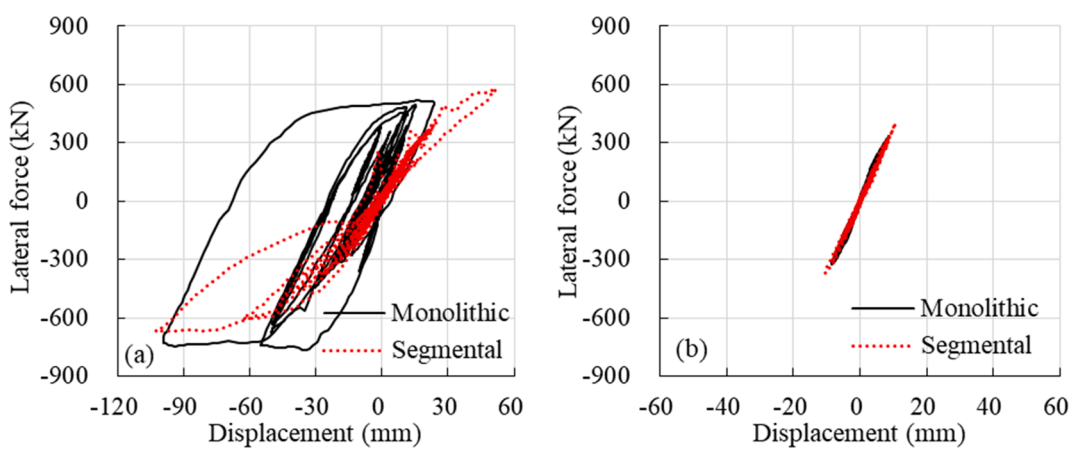

Fig. 11. Hysteretic curves of the bridge piers under (a) TCU079, ChiChi and (b) CHI012, Imperial Valley.

$$\beta_{D|IM} = \sqrt{\frac{\sum_{i=1}^{N}\left[ln(EDP_i) - ln\left(aIM_i^b\right)\right]^2}{N-2}} \tag{11}$$

in which N represents the simulation numbers.

The piers and bearings are considered as the most critical components in a bridge [68,69]. Four different damage states are used to identify the damage of the bridge components in this study [70]. Considering the self-centering property of segmental UHPC columns, the residual drift, R_Δ, is taken as the damage indicator of the piers. Lateral displacement, δ, is used to characterize the damage of the expansion bearings. The limit states of the bridge piers and bearings are tabulated in Table 5 [2,71].

The system-level fragility of the bridge can be derived from the fragilities of each component, $P[F_i]$, as shown in Equation (12). The system fragility functions, P_s, are calculated using first-order reliability theory [68,72]. The upper bound is used to conservatively evaluate the system fragility.

Table 5
Limit states of bridge components and downtime.

Limit states	Pier	Bearing	Downtime
	R_Δ (%)	δ (mm)	d (days)
Slight	0.25	50	7
Moderate	0.75	100	30
Extensive	1.00	150	120
Collapse	1.50	255	400

$$\max_{i=1}^{n}(P[F_i]) \leqslant P_S \leqslant 1 - \prod_{i=1}^{n}(1 - P[F_i]) \tag{12}$$

7.1. Probabilistic seismic demand models (PSDM)

To compare and evaluate the vulnerability of the two bridge structures, the PSDM of the bearing and pier is first developed using a scaling approach. Fig. 12 illustrates the PSDMs of the monolithic RC and segmental UHPC columns in the two bridge structures for residual displacement. For brevity, the PSDMs of the bearings are not shown here. The coefficients a and b in Eq. (10) are determined from the regression analysis. The values of a and b for the monolithic column are 0.406 and 2.359, respectively. For the segmental UHPC column, the values of a and b are 0.094 and 1.437, respectively. Similar to the columns, the corresponding values of a and b for the bearings in the conventional and novel bridges are 145.5 and 1.527, and 138.5 and 1.416, respectively. It can be observed from each plot that the relation between the EDP (i.e. R_Δ and δ) and IM (i.e. PGA) is nearly linear due to the high values of the R^2 (more than 0.65).

7.2. Fragility curves of the two bridge systems

The fragility curves of the bridge components (i.e. pier and bearing) are established based on Eq. (10). The fragility functions of the bridge components are combined to generate the system-level fragility curves using Eq. (12), as shown in Fig. 13.

Compared to the monolithic bridge, the system-level fragilities indicate that the bridge supported with segmental UHPC columns possesses less vulnerability for all the damage states. Fig. 13a shows that the two bridge systems have almost the same vulnerability at the slight damage state. However, at higher damage states, the monolithic bridge has higher damage probabilities. Fig. 13 reveals that at low PGA values, the probabilities of reaching each damage level for the segmental bridge are slightly higher in comparison to the monolithic bridge. This can be explained as follows. Since at low intensities, both the monolithic and segmental UHPC bridge piers are in the elastic range or experience very limited damage, the residual drift of the segmental pier is slightly less than or close with that of the monolithic pier. However, because of the lower ED capacity of the segmental UHPC column, the displacement of the bearings for the segmental bridge is larger than that of the bearings for the monolithic bridge. The increase of the fragility in the bearing outweighs the fragility reduction in the segmental UHPC pier, which explains the slightly higher vulnerability of the bridge with the segmental UHPC pier at the low PGA level.

At high intensities, the damage probabilities of the segmental bridge are smaller than those of the monolithic bridge. Their difference presents an increase trending as the PGA increases. The phenomenon can be attributed to the following reasons. Regarding the high PGA level, the yielding of the longitudinal steel rebars and the damage of the concrete cause the stiffness degradation of the RC pier in the monolithic bridge due to the nonlinear behavior and consequently, the peak and residual displacement of the bearing and pier increases. However, due to its high damage tolerance property, the concrete damage and stiffness degradation are not observed in the segmental UHPC pier (see Fig. 1). Besides, considering the superior self-centering capacity, the segmental pier can recover its original shape with small residual drift after an earthquake. The excellent re-centering capacity of the segmental UHPC pier renders the segmental bridge less vulnerable. For example, when PGA value is 1.0 g, there is a chance of 82.3% for the monolithic bridge to experience moderate damage, whereas the segmental bridge has a 73.3% probability (11% reduction) at the same damage level. At the collapse damage state, the fragilities of the segmental bridge are 29.3%, 33.8%, and 32.6% smaller than those of the monolithic bridge for PGA values of 1.0 g, 1.5 g, and 2.0 g, respectively. The results indicate that segmental UHPC piers should be used in high seismicity regions, which are subjected to destructive earthquakes for obtaining the benefits of using segmental UHPC piers. Another finding is that segmental UHPC piers experience very low damage probabilities at four damage states and a much higher probability of damage for the bearings is observed in the case of the segmental bridge. For brevity, the fragility curves of the two bridge components (pier and bearing) are not provided in this section. At the four damage states, the damage probabilities of the segmental column are 0.487, 0.143, 0.095, and 0.049, respectively for a PGA value of 2.0 g. Hence, restraining devices are necessary to limit the displacement response for further enhancing the seismic performance of the segmental bridge. Further research will be conducted to propose efficient restraining devices and their design methods for segmental bridges in future studies.

8. Performance-based long-term assessment

8.1. Methodology of long-term loss assessment

In this section, five different hazard scenarios are identified to estimate the lifetime loss of the two bridge structures. The considered hazard events have five different levels of seismic intensities. The return periods range from 225 (Event 1) to 5000-year (Event 5). Events 2, 3, and 4 have return periods of 475-year, 975-year, and 2475-year, respectively. The selected events can cover the earthquake intensities from low to high levels at the location of the bridge. The lower-level hazard event represents a frequent earthquake with low seismic intensity, while the upper-level event refers to a destructive earthquake with high intensity during the lifetime of a structure. The low-intensity event has a high probability of occurrence, while the occurrence

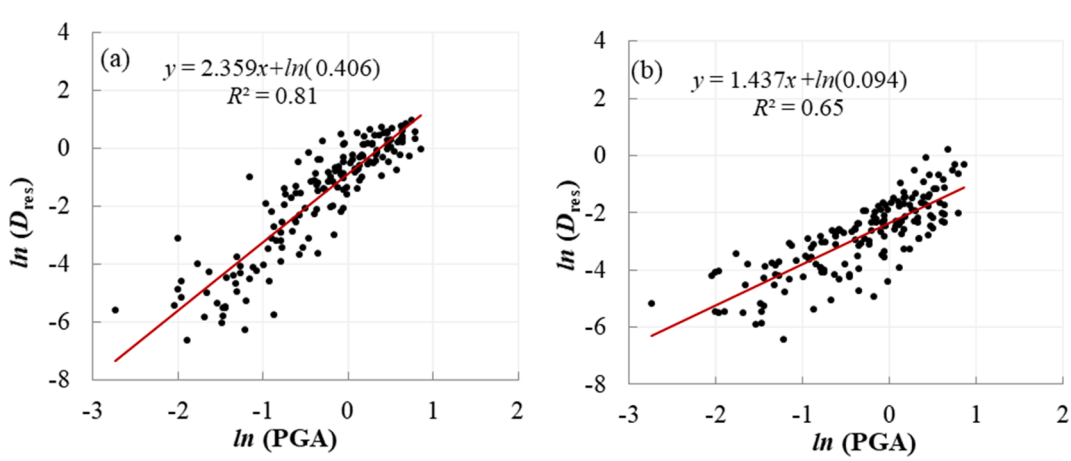

Fig. 12. Comparison of the PSDMs for the (a) segmental UHPC column and (b) monolithic column.

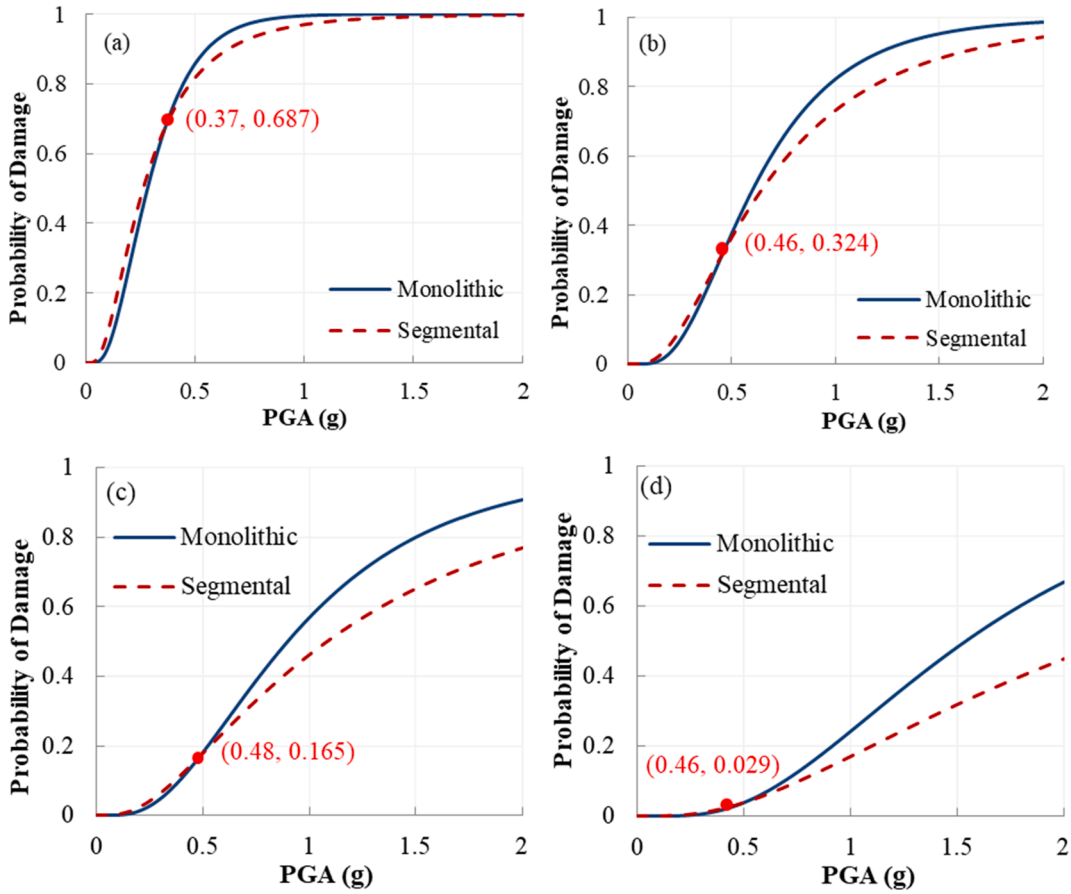

Fig. 13. Comparison of the fragility curves for the two bridge systems at (a) slight, (b) moderate, (c) extensive and (d) collapse damage state.

probability of the high-intensity event is much lower. According to CHBDC (2014) [60], the design event (DE) refers to the earthquake with a 2475-year return period (Event 4). The USGS national seismic hazard map [64] is used to determine the PGA values of the considered seismic events, which are 0.1987, 0.2935, 0.4037, 0.5823, and 0.7514 g, respectively.

Long-term seismic loss associated with the prototype and self-centering bridges is quantified to compare their performance considering repair cost and indirect loss. Here, a framework used in [73] is considered in this study. Given a hazard scenario, the expected annual loss of a bridge, L_i, can be calculated depending on the failure probability of the bridge, $P_{DS,i|PGA}$.

$$L_i = \sum_{i=1}^{4} C_{DS,i} P_{DS,i|PGA} \tag{13}$$

in which $C_{DS,i}$ is the considered direct and indirect consequences. The direct consequence (i.e. repair cost, $C_{REP,i}$) of the bridge is calculated depending on the reconstruction cost, c_{reb}, and dimension (width, W, and length, L) of the bridge [74].

$$C_{REP,i} = R_{rcr} \cdot c_{reb} \cdot W \cdot L \tag{14}$$

The values of the repair cost ratio, R_{rcr}, associated with four different damage levels are 0.1 (slight), 0.3 (moderate), 0.75 (extensive), and 1.0 (collapse), respectively [75]. Two main indirect losses (running cost, C_R, and monetary time cost, C_T) can be computed depending on the unit cost in the downtime [55]. Under a certain damage state, C_R and C_T are determined as [73,74].

$$C_{R,i} = \left[c_{R,car}\left(1 - \frac{T_0}{100}\right) + c_{R,truck}\frac{T_0}{100} \right] \cdot D_l \cdot ADT \cdot d_i \tag{15}$$

$$C_{T,i} = \left[c_{AW} o_{car}\left(1 - \frac{T_0}{100}\right) + \left(c_{ATC} o_{truck} + c_{goods}\right)\frac{T_0}{100} \right] \cdot \left[\frac{D_l \cdot ADT}{S} + ADTE \cdot \left(\frac{l}{S_D} - \frac{l}{S_0}\right) \right] d_i \tag{16}$$

The detailed explanation and the corresponding value for each parameter in Eqs. (15) and (16) are listed in Table 6. The downtimes of the prototype bridge are 7, 30, 120, and 400 days at four different damage states (see Table 5) [73]. In comparison to the cast-in-place columns, the precast columns can noticeably reduce the construction time. However, the additional construction time is needed for assembling the segments and applying the prestressed load for the post-

Table 6
Parameters associated with consequences.

Parameters	Notation	Value	References
Average daily traffic	ADT	19750	[76]
Average daily traffic on the damaged link to average daily traffic	ADTE/ ADT	0.12	[77]
Daily truck traffic ratio	T_0	13%	[78]
Link length (km)	l	6	[78]
Detour additional distance (km)	D_l	2	[78]
Vehicle occupancies for cars	o_{car}	1.5	[74,79]
Vehicle occupancies for trucks	o_{truck}	1.05	[74,79]
Wage for car drivers ($/h)	c_{AW}	11.91	[74,79]
Compensation for truck drivers ($/h)	c_{ATC}	29.87	[74,79]
Operating costs for cars ($/km)	$c_{Run,car}$	0.4	[74,79]
Operating costs for trucks ($/km)	$c_{Run,truck}$	0.57	[74,79]
Rebuilding costs ($/m^2)	c_{reb}	2306	[75]
Detour speed (km/h)	S	50	[79]
Link speed (km/h)	S_0	80	[79]
Time value of a cargo ($/h)	c_{goods}	4	[77]
Monetary discount rate	τ	0.035	[55]

tensioned column. Therefore, to be conservative, a 20% shorter restoration time (downtime) is assumed for the bridge with the segmental UHPC piers, i.e., the downtimes of the precast segmental bridge are 6, 24, 96, and 320, respectively.

The total life-cycle loss, $LCL(t_{\text{int}})$, is expressed as [55].

$$LCL_i(t_{int}) = \sum_{i=1}^{N(t_{int})} L_i(t_k)\cdot e^{-\tau t_k} \tag{17}$$

where $N(t_{\text{int}})$ denotes the earthquake numbers in the time interval, t_{int}; $L_i(t_k)$ denotes the expected annual seismic loss at time t_k; τ denotes the discount rate of the money. The total expected loss, $E[LCL(t_{\text{int}})]$, can be calculated as follows [55].

$$E[LCL_i(t_{int})] = \frac{\lambda_f \cdot E(L_i)}{\tau}\cdot(1 - e^{-\tau\cdot t_{int}}) \tag{18}$$

To comprehensively understand the long-term performance of the innovative bridge system, the indirect loss is assessed in this study. However, numerous factors may directly influence the calculation of indirect consequences, such as the bridge location, traffic flow across the bridge changing with time, variation of damaged link length in the transportation network, etc. Since many parameters in the assessment procedure may change with the level of the economics, the strategy of the repair (e.g. downtime, detour selection), etc., a more accurate indirect loss can be easily calculated after knowing more relevant information following the above framework.

8.2. Long-term loss analysis

Equations 14–16 are used to calculate the costs of direct and indirect consequences. Then, the expected annual loss, L_i, is derived using Equation (13). The relevant parameters associated with the consequences are tabulated in Table 6.

The direct and indirect losses for the two bridge structures are depicted in Fig. 14a and b. It can be observed that both the direct and indirect losses show an increase trending as the seismic intensity increases. From Event 1 to Event 3, the segmental bridge results in a larger seismic loss. This is because, under low-level earthquakes, both the monolithic and segmental bridge piers experience negligible residual drift after an earthquake; however, the use of segmental piers leads to a greater deformation of the bearing. More explanation has been provided in the above analysis. Under Events 4 and 5, the segmental UHPC piers make the bridge experience less direct and indirect losses due to the high damage tolerance and excellent self-centering capacity. For the design event (i.e. Event 4), the direct and indirect losses of the bridge supported by the segmental UHPC piers decrease by 7.1% and 13.6%, respectively in comparison to the monolithic bridge. Under the maximum considered event (MCE, Event 5), the segmental UHPC piers cause about 7.8% and 16.5% in the direct and indirect losses, respectively. Besides, it is found that the indirect consequences may cause higher seismic losses compared to the direct consequence.

After calculating the direct and indirect losses, the expected total loss of the monolithic and segmental bridges under a given t_{int} and τ can be computed using Eq. (18). In this study, it is assumed that t_{int} and τ are 75 years and 2%, respectively. Fig. 14c illustrates the expected life-cycle losses of the two bridge structures under the five hazard scenarios. It can be seen that Event 2 causes the maximum life-cycle seismic loss among the five events. The same phenomenon is observed in the study of Zheng and Dong [54]. Similar to the direct and indirect losses, the segmental bridge experiences lower expected life-cycle loss compared to that of the monolithic bridge under Events 4 and 5. Due to the lower occurrence probability of Event 4, the expected long-term loss under Event 4 with low seismic intensity is higher than that under Event 5. For the DE (Event 4) and MCE (Event 5), the expected long-term losses of the segmental bridge are about 45,673 USD and 33,918 USD, which are approximately 92% and 84% of that of the monolithic bridge,

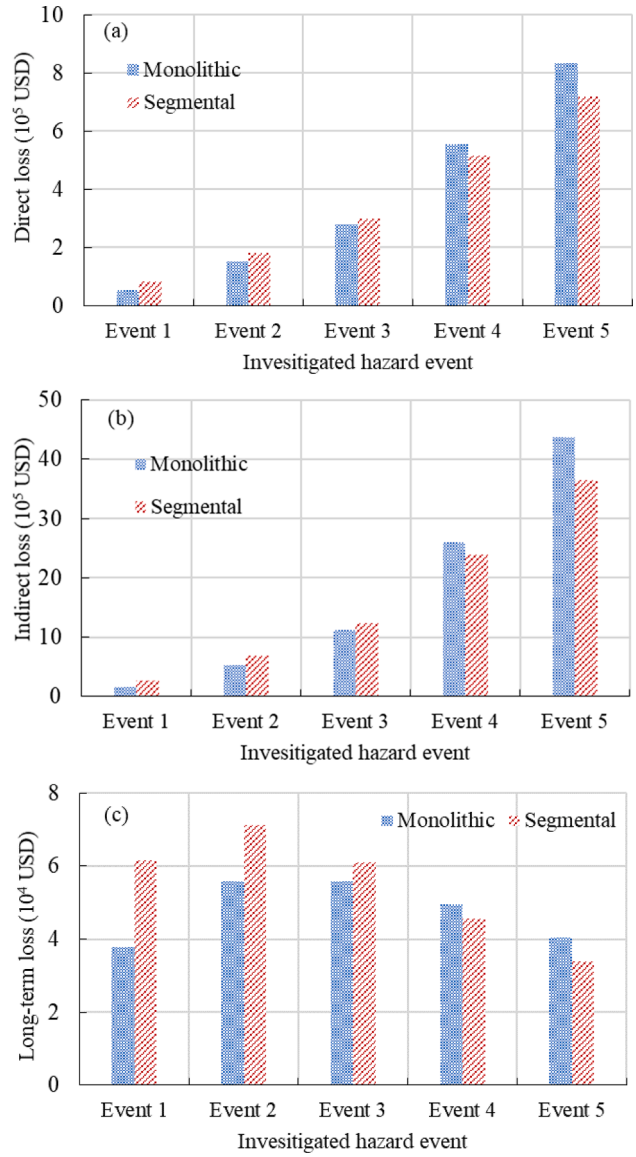

Fig. 14. Direct, indirect and long-term loss of the bridges under the five hazard events (a) direct cost, (b) indirect cost, and (c) expected long-term loss at given $t_{\text{int}} = 75$ years and $\tau = 0.02$.

respectively. The results indicate that the bridge supported by segmental UHPC piers is more economically beneficial under destructive earthquakes with a low occurrence probability. To thoroughly understand the influence of the return period, the variations of the expected long-term loss with a wide range of return periods are presented in Fig. 15. It can be seen that when the return period exceeds 1500 years, the segmental bridge results in a less long-term loss.

9. Conclusions

The application of bridge systems with precast segmental columns has been widely promoted in engineering practices. Conventional segmental RC columns have good self-centering property, but their damage tolerance and energy dissipation capacity are still limited. Recently, precast segmental UHPC columns have been proposed and can efficiently overcome the above limitations according to the numerical and experimental studies by the authors. Although the cyclic response of such bridge columns has been experimentally investigated, the effects of precast segmental UHPC columns on the overall performance of a whole bridge at system level are not yet well understood. Besides, because of

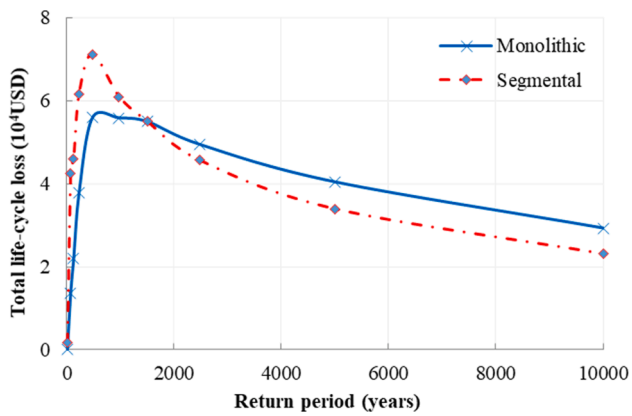

Fig. 15. Variations of the expected long-term loss with the return period of seismic events.

the high initial cost of UHPC materials, the application of such a column is rare. To close the gap, this study performs numerical studies on the long-term performance of a benchmark bridge with precast segmental UHPC columns. A design procedure is proposed to properly design the segmental UHPC column with a hollow section for the bridge. A new type of UHPC material with river sand and coarse aggregate is used to manufacture these specimens for reducing its cost and promoting its application. The concluding remarks are summarized.

1. Compared with the monolithic RC column, the precast segmental UHPC column showed smaller residual drift. The stiffness degradation could be efficiently avoided due to the high damage tolerance capacity of UHPC materials and superior self-centering property of post-tensioned tendons. Using UHPC replace of convention RC could make the bridge column more reliable.
2. A design procedure was developed to design the segmental column for ensuring similar stiffness and strength with the monolithic column. The bridge supported by the designed columns experienced almost the same peak acceleration with the monolithic bridge. Consequently, it could provide an alternative tool for designing segmental columns.
3. From the seismic analysis, it was observed that the segmental UHPC columns possessed good self-centering capacity and could effectively reduce its residual deformation. Compared with the monolithic bridge, the residual drift of both the deck and pier decreased by above 80%, whereas the peak drift demand of the deck and pier increased by about 17% under the selected near fault records due to the lower energy dissipation capacity of segmental UHPC column. Replacing monolithic columns with segmental UHPC columns could cause a 19% increase in self-centering ratio (SCR), but a 42% reduction in energy dissipation.
4. From the fragility analysis, with respect to the high PGA level, a significant reduction in the vulnerability was observed when segmental UHPC piers replace monolithic piers. This could be attributed to the negligible concrete damage and good self-centering capacity of segmental UHPC piers. The bridge bearings experienced much higher damage probabilities than the segmental UHPC columns due to a lack of restraining devices.
5. By using segmental UHPC columns, the initial construction cost of the bridge increased by about 2.6%. The UHPC segmental columns were more economically viable in high seismic regions. For instance, the expected long-term losses of the segmental bridge under design event (DE) and maximum considered event (MCE) were approximate 92% and 84% of that of the monolithic bridge, respectively. Another finding was that when the return period exceeded 1500 years, the segmental bridge resulted in a smaller long-term loss.

The long-term performance assessment is developed according to the fragility functions. The uncertainties, such as material and geometric properties of the bridge, IMs, location, will be considered to accurately estimate the seismic performance of the bridge supported by segmental UHPC columns. Besides, the curvature or displacement ductility is usually regarded as the EDP of RC piers. However, there is a lack of relevant studies on the damage states of the segmental bridge piers considering curvature or displacement ductility as EDP, which warrants further research. In this study, the proposed model has been validated against a series of experimental results. The model can accurately predict the initial yield, fracture of the ED bars, and the joint opening. However, since the shake table tests on the seismic responses of a bridge supported by the segmental piers are still limited, the authors did not compare the numerical results with the test results obtained from shake table tests. The authors are planning to perform shake table tests on such bridge piers in near future. Further validation of the numerical model with a shake table test will be conducted to investigate the seismic responses of a bridge system with segmental piers in a future study.

CRediT authorship contribution statement

Shuai Li: Conceptualization, Methodology, Software, Formal analysis, Writing - original draft, Writing - review & editing, Visualization, Funding acquisition. **Taiyi Zhao:** Methodology, Investigation, Software. **M. Shahria Alam:** Conceptualization, Supervision, Writing - review & editing, Supervision, Project administration, Funding acquisition. **Zhao Cheng:** Validation, Writing - review & editing. **Jing-quan Wang:** Conceptualization, Supervision, Project administration, Funding acquisition.

Declaration of competing interest

The authors declared no potential conflicts of interest with respect of to the research, authorship, and/or publication of this article.

Acknowledgments

This study was financially supported by the National Natural Science Foundation of China (Grant No. 51908123 and U1934205), the Fundamental Research Funds for the Central Universities (Grant No. 2242020K40091), the Natural Science Foundation of Jiangsu Province (Grant No. BK20190370), and Natural Sciences and Engineering Research Council (NSERC) of Canada through Discovery Grant.

References

[1] Kawashima K, MacRae G, Hoshikuma J, Nagaya K. Residual displacement response spectrum. J Struct Eng ASCE 1998;124:523–30.
[2] Billah AHMM, Alam MS. Seismic fragility assessment of concrete bridge pier reinforced with superelastic shape memory alloy. Earthq Spectra 2015;31(3):1515–41.
[3] Ramirez CM, Miranda E. Significance of residual drifts in building earthquake loss estimation. Earthq Eng Struct Dynam 2012;41(11):1477–93.
[4] Shrestha B, Li C, Hao H, et al. Performance-based seismic assessment of superelastic shape memory alloy-reinforced bridge piers considering residual deformations. J Earthq Eng 2017;21(7):1050–69.
[5] Kwan WP, Billington SL. Unbonded posttensioned concrete bridge piers. I: Monotonic and cyclic analyses. J Bridge Eng ASCE 2003;8(2):92–101.
[6] Saiidi MS, O'Brien M, Sadrossadat-Zadeh M. Cyclic response of concrete bridge columns using superelastic nitinol and bendable concrete. ACI Struct 2009;106(1):69–77.
[7] Ou YC, Wang PH, Tsai MS, et al. Large-scale experimental study of precast segmental unbonded posttensioned concrete bridge columns for seismic regions. J Struct Eng ASCE 2009;136(3):255–64.
[8] Zhang Q, Alam MS. Evaluating the seismic behavior of segmental unbounded posttensioned concrete bridge piers using factorial analysis. J Bridge Eng ASCE 2015;21(4):04015073.
[9] Ou YC, Pratiwi AY, Song J. Pseudodynamic testing and inelastic displacement ratios of self-centering precast concrete segmental bridge columns. J Struct Eng ASCE 2018;144(9):04018158.

[10] Wang Z, Wang JQ, Liu TX, et al. An explicit analytical model for seismic performance of an unbonded post-tensioned precast segmental rocking hollow pier. Eng Struct 2018;161:176–91.
[11] Yang C, Okumus P. Ultrahigh-performance concrete for posttensioned precast bridge piers for seismic resilience. J Struct Eng ASCE 2017;143(12):04017161.
[12] Wang Z, Wang J, Zhu J, et al. Energy dissipation and self-centering capacities of posttensioning precast segmental ultra-high performance concrete bridge columns. Struct Concr 2019:1–16.
[13] Mander JB, Cheng CT. Seismic resistance of bridge piers based on damage avoidance design. Report no. NCEER-97-0014. State University of New York, Buffalo; 1997.
[14] Zhu Z, Ahmad I, Mirmiran A. Seismic performance of concrete-filled FRP tube columns for bridge substructure. J Bridge Eng ASCE 2006;11(3):359–70.
[15] Chou CC, Chen YC. Cyclic tests of post-tensioned precast CFT segmental bridge columns with unbonded strands. Earthq Eng Struct Dynam 2006;35(2):159–75.
[16] Wang JC, Ou YC, Chang KC, et al. Large-scale seismic tests of tall concrete bridge columns with precast segmental construction. Earthq Eng Struct Dynam 2008;37(12):1449–65.
[17] ElGawady MA, Sha'lan A. Seismic behavior of self-centering precast segmental bridge bents. J Bridge Eng ASCE 2010;16(3):328–39.
[18] Motaref S, Saiidi MS, Sanders D. Shake table studies of energy-dissipating segmental bridge columns. J Bridge Eng ASCE 2013;19(2):186–99.
[19] Billington SL, Yoon JK. Cyclic response of unbonded posttensioned precast columns with ductile fiber-reinforced concrete. J Bridge Eng ASCE 2004;9(4):353–63.
[20] Marriott D, Pampanin S, Palermo A. Quasi-static and pseudo-dynamic testing of unbonded post-tensioned rocking bridge piers with external replaceable dissipaters. Earthq Eng Struct Dynam 2009;38(3):331–54.
[21] Solberg K, Mashiko N, Mander JB, et al. Performance of a damage-protected highway bridge pier subjected to bidirectional earthquake attack. J Struct Eng ASCE 2009;135(5):469–78.
[22] Trono W, Jen G, Panagiotou M, et al. Seismic response of a damage-resistant recentering posttensioned-HYFRC bridge column. J Bridge Eng ASCE 2014;20(7):04014096.
[23] Palermo A, Pampanin S, Marriott D. Design, modeling, and experimental response of seismic resistant bridge piers with posttensioned dissipating connections. J Bridge Eng ASCE 2007;133(11):1648–61.
[24] Kam WY, Pampanin S, Palermo A, et al. Self-centering structural systems with combination of hysteretic and viscous energy dissipations. Earthq Eng Struct Dynam 2010;39(10):1083–108.
[25] Ou YC, Tsai MS, Chang KC, et al. Cyclic behavior of precast segmental concrete bridge columns with high performance or conventional steel reinforcing bars as energy dissipation bars. Earthq Eng Struct Dynam 2010;39(11):1181–98.
[26] Marriott D, Pampanin S, Palermo A. Biaxial testing of unbonded post-tensioned rocking bridge piers with external replaceable dissipaters. Earthq Eng Struct Dynam 2011;40(15):1723–41.
[27] Bu ZY, Ou YC, Song JW, et al. Cyclic loading test of unbonded and bonded posttensioned precast segmental bridge columns with circular section. J Bridge Eng ASCE 2015;21(2):04015043.
[28] Guo T, Cao Z, Xu Z, et al. Cyclic load tests on self-centering concrete pier with external dissipators and enhanced durability. J Struct Eng ASCE 2015;142(1):04015088.
[29] Moon DY, Roh H, Cimellaro GP. Seismic performance of segmental rocking columns connected with NiTi martensitic SMA bars. Adv. Struct Eng 2015;18(4):571–84.
[30] Wang CL, Gao Y, Cheng X, et al. Experimental investigation on H-section buckling-restrained braces with partially restrained flange. Eng Struct 2019;199:109584.
[31] Graybeal BA. Compressive behavior of ultra-high-performance fiber-reinforced concrete. ACI Mater J 2007;104(2):146.
[32] Graybeal B, Tanesi J. Durability of an ultrahigh-performance concrete. J Mater. Civil Eng. 2007;19(10):848–54.
[33] Baby F, Graybeal B, Marchand P, et al. Proposed flexural test method and associated inverse analysis for ultra-high-performance fiber-reinforced concrete. ACI Mater J 2012;109(5):545.
[34] Ichikawa S, Matsuzaki H, Moustafa A, et al. Seismic-resistant bridge columns with ultrahigh-performance concrete segments. J Bridge Eng ASCE 2016;21(9):04016049.
[35] Sugano S, Kimura H, Shirai K. Study of New RC structures using ultra-high-strength fiber-reinforced concrete (UFC). J Adv Concrete Technol 2007;5(2):133–47.
[36] Kimura H, Ishikawa Y, Kambayashi A, et al. Seismic behavior of 200 MPa ultra-high-strength steel-fiber reinforced concrete columns under varying axial load. J Adv Concrete Technol 2007;5(2):193–200.
[37] Ousalem H, Takatsu H, Ishikawa Y, et al. Use of high-strength bars for the seismic performance of high-strength concrete columns. J Adv Concrete Technol 2009;7(1):123–34.
[38] Zohrevand P, Mirmiran A. Cyclic behavior of hybrid columns made of ultra high performance concrete and fiber reinforced polymers. J Compos Constr 2011;16(1):91–9.
[39] Zohrevand P, Mirmiran A. Effect of column parameters on cyclic behavior of ultra-high-performance concrete-filled fiber-reinforced polymer tubes. ACI Struct J 2013;110(5):823.
[40] Tazarv M, Saiid MS. Low-damage precast columns for accelerated bridge construction in high seismic zones. J Bridge Eng ASCE 2015;21(3):04015056.
[41] Tazarv M, Saiidi MS. UHPC-filled duct connections for accelerated bridge construction of RC columns in high seismic zones. Eng Struct 2015;99:413–22.
[42] Mohebbi A, Saiidi MS, Itani AM. (2017) Seismic design of precast piers with pocket connections, CFRP tendons, and ECC/UHPC columns. Int J Bridge Eng Spec 2017;2017:99–123.
[43] Binard JP. UHPC: a game-changing material for PCI bridge producers. PCI J 2017;62(2):34–46.
[44] Sideris P, Aref AJ, Filiatrault A. Large-scale seismic testing of a hybrid sliding-rocking posttensioned segmental bridge system. J Struct Eng ASCE 2014;140(6):04014025.
[45] Zhao L, Bi K, Hao H, et al. Numerical studies on the seismic responses of bridge structures with precast segmental columns. Eng Struct 2017;151:568–83.
[46] Lee WK, Billington SL. Performance-based earthquake engineering assessment of a self-centering, post-tensioned concrete bridge system. Earthq Eng Struct Dynam 2011;40(8):887–902.
[47] Wang J, Wang Z, Tang Y, et al. Cyclic loading test of self-centering precast segmental unbonded posttensioned UHPFRC bridge columns. B Earthq Eng 2018;16(11):5227–55.
[48] Wang Z, Wang JQ, Xiu HL, et al. Equivalent plastic hinge model of rectangular hollow piers. China Highway Trans 2019;32(1):76–85.
[49] Liu J, Han F, Cui G, et al. Combined effect of coarse aggregate and fiber on tensile behavior of ultra-high performance concrete. Constr Build Mater 2016;121:310–8.
[50] McKenna F, Fenves GL, Scott MH. Open System for Earthquake Engineering Simulation (OpenSees). Berkeley, CA: University of California (http://opensees.berkeley.edu); 2000.
[51] Si BJ, Gu MY, Sun ZG, Du M. Seismic response analysis of the rocking self-centering bridge piers under the near-fault ground motions. Eng Mech 2017;34(10):87–97.
[52] Sun ZG, Zhao TY, Shi Y, Wang DS. Research on numerical modeling method for rocking self-centering bridge piers. J Basic Sci Eng 2020;27(6):1357–69.
[53] ElGawady MA, Sha'lan A. Seismic behavior of self-centering precast segmental bridge bents. J Bridge Eng ASCE 2011;16(3):328–39.
[54] Zheng Y, Dong Y. Performance-based assessment of bridges with steel-SMA reinforced piers in a life-cycle context by numerical approach. B Earthq Eng 2019;17(3):1667–88.
[55] Zheng Y, Dong Y, Li Y. Resilience and life-cycle performance of smart bridges with shape memory alloy (SMA)-cable-based bearings. Constr Build Mater 2018;158:389–400.
[56] Siddiquee K, Alam M. Highway bridge infrastructure in the province of British Columbia (BC), Canada. Infrastruct 2017;2(2):7.
[57] Caltrans. Seismic design criteria. Sacramento, CA; 2013.
[58] FHWA (Federal Highway Administration). Seismic Retrofitting Manual for Highway Structures: Part 1-Bridges. U.S. Dept. of Transportation, Washington, DC; 2006.
[59] Xu LQ, Li JZ. Experiment on seismic performance and its improvement of reinforced concrete retainers. China J Highway Transport 2014;27(9):41–8 [in Chineses].
[60] Canadian Standards Association. CAN/CSA-S6-14—Canadian highway bridge design code. Rexdale, Ontario, Canada: Canadian Standards Association; 2014.
[61] Sakai J, Mahin S. Analytical investigations of new methods for reducing residual displacements of reinforced concrete bridge columns. PEER Report 2004/02, Pacific Earthquake Engineering Research Center, University of California, Berkeley, CA, 2004.
[62] Hedayati Dezfuli F, Li S, Alam MS, et al. Effect of constitutive models on the seismic response of an SMA-LRB isolated highway bridge. Eng Struct 2017;148:113–25.
[63] Naumoski N, Tso WK, Heidebrecht AC. A selection of representative strong motion earthquake records having different A/V ratios. EERG Report 88-01, Earthquake Engineering; 1988.
[64] Li S, Zhang F, Wang JQ, Zhang J, Alam MS. Effects of near-fault motions and artificial pulse-type ground motions on super-span cable-stayed bridge systems. J Bridge Eng ASCE 04016128; 2017.
[65] Li S, Hedayati Dezfuli F, Wang J, Alam MS. (2020) Performance-based seismic loss assessment of isolated simply-supported highway bridges retrofitted with different shape memory alloy cable restrainers in a life-cycle context. J Intel Mat Syst Struct 2020;31(8):1053–75.
[66] USGS 2017 Unified hazard tool (https://earthquake.usgs.gov/hazards/interactive/).
[67] Padgett JE, DesRoches R. Bridge functionality relationships for improved seismic risk assessment of transportation networks. Earthq Spectra 2007;23(1):115–30.
[68] Hedayati Dezfuli F, Alam MS. Seismic vulnerability assessment of a steel-girder highway bridge equipped with different SMA wire-based smart elastomeric isolators. Smart Mater Struct 2016;25(7):075039.
[69] Xie Y, Zhang J. Optimal design of seismic protective devices for highway bridges using performance-based methodology and multiobjective genetic optimization. J Bridge Eng ASCE 2016;22(3):04016129.
[70] HAZUS, Multi-hazard loss estimation methodology earthquake model. Technical Manual. Department of Homeland Security Emergency Preparedness and Response Directorate FEMA Mitigation Division, Washington, D.C., 2003.
[71] Choi E, DesRoches R, Nielson B. Seismic fragility of typical bridges in moderate seismic zones. Eng Struct 2004;26(2):187–99.
[72] Zhang J, Huo Y. Evaluating effectiveness and optimum design of isolation devices for highway bridges using the fragility function method. Eng Struct 2009;31:1648–60.
[73] Dong Y, Frangopol DM, Saydam D. Time-variant sustainability assessment of seismically vulnerable bridges subjected to multiple hazards. Earthq Eng Struct Dyn 2013;42(10):1451–67.
[74] Stein SM, Young GK, Trent RE, Pearson DR. Prioritizing scour vulnerable bridges using risk. J Infrastruct Syst 1999;5(3):95–101.

[75] Mander JB. Fragility curve development for assessing the seismic vulnerability of highway bridges. Technical Rep., Univ. at Buffalo, State University of New York, NY; 1999.
[76] Dong Y, Frangopol DM. Risk and resilience assessment of bridges under mainshock and aftershocks incorporating uncertainties. Eng Struct 2015;83:198–208.
[77] Decò A, Frangopol DM. Risk assessment of highway bridges under multiple hazards. J Risk Res 2011;14(9):1057–89.
[78] FHWA (Federal Highway Administration) (2015) National bridge inventory (NBI) database. U.S. Dept. of Transportation, Washington, DC.
[79] Dong Y, Frangopol DM. Probabilistic time-dependent multihazard life-cycle assessment and resilience of bridges considering climate change. J Perform Constr Fac 2016;30(5):1–12.